Framework water capacity and infiltration pressure of MFI zeolites

Framework Water Capacity and Infiltration Pressure of MFI Zeolites

Thomas Humplik[a], Rishi Raj[a], Shalabh C. Maroo[b], Tahar Laoui[c], and Evelyn N. Wang[a,*]

[a]Department of Mechanical Engineering, Massachusetts Institute of Technology, Cambridge MA 02139
[b]Department of Mechanical & Aerospace Engineering, Syracuse University, Syracuse NY 13244
[c]Department of Mechanical Engineering, King Fahd University of Petroleum and Minerals, Dhahran, Saudi Arabia

* Corresponding Author: Tel: +1 617 324 3311, email: enwang@mit.edu (E. N. Wang)
77 Massachusetts Avenue, 3-461, Cambridge, MA 02139

Abstract

The high specific surface area and sub-nanometer to nanometer pore dimensions of microporous materials (pores <2 nm) can be exploited to improve a variety of applications such as separation technologies, energy storage, and fuel cells. For example, the ≈5.5 Å diameter pore of MFI (Mobil Five) zeolites has been proposed as a molecular sieve for water-based separation techniques. However, results from past experimental and simulation studies have been inconsistent, even for basic quantities such as the framework water capacity and the pressure at which the MFI zeolite pores become water-saturated (infiltration pressure). In this work, we elucidate the underlying mechanisms behind such discrepancies *via* combined water adsorption and high-pressure infiltration (or intrusion) experiments on various MFI zeolites where the characteristic crystal dimension was varied from nano (≈ 10 nm) to micro (≈ 10 μm) scales. Detailed characterization techniques were utilized to demonstrate the presence of non-crystalline silica regions in

<100 nm zeolites. Accordingly, an estimated decrease of up to 50% in the framework water capacity was observed for these zeolites when compared to the fully-crystallized larger zeolites, where 35 ± 2 water molecules were required to saturate a unit cell. On the other hand, the water infiltration pressure for all of the zeolites was ≈95 – 100 MPa despite the differences in the synthesis procedure, indicating uniformity in the crystallized pore structure and surface chemistry. These results are an essential first step towards investigating water transport mechanisms within the sub-nanometer pores and can be used to validate and improve upon existing molecular simulations in order to obtain design guidelines for practical applications such as water-based separation technologies.

Keywords

MFI Zeolite; Water Infiltration; Adsorption; Textural Porosity; Hydrophobicity

1. Introduction

The substantial increase in the surface area to volume ratio along with the change in physical properties that a material exhibits at sub-nanometer and nanometer length scales are two of the main reasons behind the growing interest in nanoscience and technology [1-6]. Of particular interest is the effect of confinement and increased surface interactions on the transport properties of water at these length scales [7-11]. If favorable, such effects can be exploited to improve the performance of desalination systems [12], molecular separation devices [13], energy recovery methods [11, 14], and fuel cells [15]. However, the scope of experimental studies investigating water transport at the nanoscale can be limited by fabrication and visualization techniques, as well as by the challenges in attaining uniform geometries over a large enough scale to obtain a measurable signal during experiments [16, 17]. As a result, the associated experimental uncertainty may be significant, which can mask the physics behind transport phenomena, and also prevent direct comparison with simulation studies. Conversely, typical simulation domains are limited by computational constraints and normally used nano-sized domains (idealized cases of a single or a few nanopores) are often not enough to capture actual experimental observations [18-22].

The high specific surface area and the uniformity in sub-nanometer pores of zeolites, a class of materials with well-known synthesis procedures [23], however, can overcome some of these challenges and offer a route to study nanoscale transport phenomena using macroscopic experimental techniques. Specifically, water transport in MFI zeolites (a silica-based microporous material with ≈5.5 Å

diameter pores), where the pore structure can be utilized as a molecular sieve for water desalination [24-26], has been studied extensively [27-38]. In spite of the advantages of uniform pore geometry, simplified synthesis, and over three decades of widespread research [23], the water infiltration mechanisms and the subsequent transport through the pores remain unclear. For example, the range of experimentally reported diffusivity values for water within purely siliceous MFI zeolites spans seven orders of magnitude, from $\approx 10^{-7}$ m^2/s - 10^{-14} m^2/s [39-43]. Furthermore, even a basic quantity such as the total framework (internal) capacity per unit cell of the MFI zeolite varies significantly (34-57 water molecules per unit cell) amongst both experiments and simulations (Table 1). Similarly, some studies show that the infiltration pressure is low (1– 30 kPa, adsorption regime, [37, 44, 45]), while others report very high values for the infiltration pressure (>30 MPa, high pressure infiltration regime [14, 46, 47]). A variation in the infiltration pressure could arise from small changes in the zeolite composition or internal defect density, however, the disagreement over the total internal water capacity, which ideally should remain consistent amongst all MFI-zeolites (so long as the internal pore structure does not undergo significant structural changes), highlights a lack of understanding of water transport within MFI-zeolites. We attribute much of this discrepancy to the unknown contribution of the textural porosity (*i.e.*, inter-crystalline pores) on the overall water uptake along with the unknown quantity of pre-adsorbed water into the pores of hydrophobic MFI zeolites.

In this work, we performed controlled experiments and detailed sample characterizations to investigate the total framework water capacity and infiltration

pressure, and identified the subtleties that may have led to the discrepancies in literature. We synthesized and procured various sizes of purely siliceous MFI-type zeolites (Silicalite-1) and confirmed the uniformity in structure and morphology using scanning electron microscopy (SEM), transmission electron microscopy (TEM), x-ray diffraction (XRD), nitrogen sorption, and nuclear magnetic resonance (NMR). Combined water adsorption and high-pressure infiltration experiments on these MFI zeolites with characteristic crystal dimensions between ≈10 nm – 10 μm were performed. The framework water capacity for fully crystalline MFI zeolites was determined to be 35 ± 2 water molecules per unit cell. Nano-sized zeolites, with crystal diameters up to 100 nm, exhibited a reduction in both the measured micropore volume (up to 25% compared to the larger zeolites) as well as the total internal water capacity (up to 50% compared to the larger zeolites). The decrease was attributed to the un-crystallized silica regions infused within the crystal resulting from incomplete synthesis. Despite the differences in synthesis procedure and crystal morphology for the various zeolites, the infiltration pressure was approximately the same, ≈95 – 100 MPa. The experimentally determined framework water capacity of 35 ± 2 water molecules per unit cell and infiltration pressure values of ≈95 – 100 MPa can now be utilized to validate and improve upon the existing water-zeolite interaction potentials used in molecular simulations. The appropriate interaction potentials can then facilitate design guidelines for practical applications such as porous membranes for water desalination.

2. Experimental

The following sections provide information on synthesis, characterization, and experimental procedures. In certain cases, further details are provided in the supplementary information as necessary.

2.1 Zeolite Synthesis

The details of the zeolite synthesis (composition, temperature, and time) are provided in Table 2. Tetraethyl orthosilicate (TEOS, Sigma Aldrich) and tetrapropylammonium hydroxide (TPAOH, 40 wt % aqueous solution, Sigma-Aldrich) were used as the silica source and the structure-directing agent (SDA), respectively. Class 2 deionized water (VWR) was used to control the pH of the synthesis solutions. Further details on each synthesis process are provided in Section S.1 of the supplementary information. Post synthesis, all zeolites were calcined at 550 °C in air to remove the precursor from the pores. The zeolites are referred to by their respective internal to external surface area ratio. For example, the ratio of internal framework surface area to outer crystal surface area for the largest crystal investigated in this study (MFI 12000 in Figure 1) is 12000. The internal surface area was estimated by calculating the available surface area of the total number of unit cells in each crystal using a geometric approximation [48] while the external surface area was estimated from the characteristic crystal dimensions directly measured using the imaging techniques described in the Section 2.2.1.

2.2 Characterization

2.2.1 Imaging

The nano-sized zeolites (Figure 1, MFI 50, 120 and 250) were imaged by transmission electron microscopy (2100, JEOL) (TEM) while the larger, micron-sized zeolites (Figure 1, MFI 1150, 1500, 12000) were imaged using scanning electron microscopy (Ultra-55, Zeiss) (SEM). For SEM analysis, the samples were coated with ≈10 nm of Pt/Pd to prevent charging during imaging. The dimensions and exterior surface area of all zeolites were determined by statistical sampling of >20 crystals. For MFI 50 and 120, the average crystal diameter estimated from these images was subsequently confirmed using x-ray diffraction techniques. Due to the variation in zeolite shapes from smaller spherical to larger prismatic crystals, the ratio of crystal volume to external surface area (in units of nanometers) was used to define the characteristic crystal dimension (Table 2) in this study.

2.2.2 X-ray diffraction (XRD)

X-ray diffraction (PANalytical X'Pert Pro, Phillips) was performed using a Cu Kα target and a nickel filter to collect the diffraction patterns (Figure 1B) and probe the crystallinity of each zeolite sample. To confirm the sizes of MFI 50 and MFI 120, Scherrer's equation [49] was utilized and the full width at half maximum of the 7.94°, 14.77°, and 22.01° peaks were obtained. The average diameter was then found by

$$d = \frac{K\lambda}{\beta cos\theta} \qquad (1)$$

where d is the crystal diameter, K is the crystal shape factor (*i.e.*, K=1 in this case), λ is the wavelength of the x-rays (for a Cu target, λ = 1.542 Å), β is the full width at half-maximum, and θ is Bragg's angle.

2.2.3 Water Adsorption and Infiltration Experiments

To quantify the amount of water that adsorbs on the zeolites up to the saturation pressure (3.14 kPa at 25 °C), physiosorption of water vapor was carried out at 25 °C using a gravimetric vapor sorption analyzer (Q5000SA, TA Instruments) (Figure 2A). Before the tests, the samples were dried in a furnace at 400 °C under air for at least 10 hours. The relative humidity was increased in steps and the calculated adsorbed water was converted into the units of water molecules per unit cell of zeolite.

A custom-built pressure vessel in a mechanical testing apparatus (Instron, 5582) was used to examine additional water infiltration within the zeolite framework at significantly higher pressures beyond the saturation pressure limit of the gravimetric vapor sorption analyzers (Figure 2B). A volumetric compression rate of ≈254 mm^3/min (corresponding to a displacement rate of 2 mm/min) was applied and the displacement and load were recorded. The compression rate was varied to ensure that transient effects did not affect the behavior. The vessel was compressed to a load of 20 kN, corresponding to a pressure of ≈160 MPa, and the displacement data was corrected for water compressibility at these high pressures. The water capacity was calculated by equating the displaced volume to an equivalent amount of water molecules entering per unit cell of the zeolites. The total capacity of the MFI zeolites was found by combining the determined adsorption and

infiltration capacities. Further details on the pressure vessel and experimental procedure can be found in Section S.2 of the supplementary information.

2.2.4 Nitrogen Sorption

The micropore volume of the zeolites was probed by carrying out physiosorption of nitrogen at 77 K (ASAP 2020, Micromeretics). The samples were dried and degassed for 5 hours at 400 °C and at a pressure of 10 μm Hg prior to the tests. The adsorption isotherms are shown in Figure 3A and the t-plot micropore volume (estimated by extrapolating the y-intercept from a linear fit in the partial pressure regions of 0.5 – 0.7) is shown in Table 3.

2.2.5 Nuclear Magnetic Resonance (NMR)

"Nuclear Magnetic Resonance (^{29}Si MAS NMR) spectra were recorded with a TMS chemical shift standard (DSX-500, Bruker) with the spectra shown in Figure 3B. ^{29}Si MAS NMR spectra (11.4 T, ω_L = 8 kHz) were acquired at 300 MHz with a recycle delay of 100 – 120 seconds with a 4 mm rotor. The spectra, shown in Figure 3B, were recorded in the frequency ranges of -97 to -107 ppm and -108 to -119 ppm to probe the quantity and quality of defect groups (*i.e.*, Q3 groups) and to probe the localized order of the silica sites (*i.e.*, Q4 groups), respectively."

3. Results and Discussion

Based on the methods described above, we first confirmed the morphology and the crystallinity of the zeolite samples. The TEM and SEM micrographs for the six zeolites synthesized/procured are shown in Figure 1A. The two smaller zeolites, *i.e.*,

MFI 50 and MFI 120, which do not have well-defined morphologies, were roughly approximated as spheres. Lattice planes were detected in >95% of the crystals examined in the TEM analysis, indicating that the majority of the samples had crystallized. MFI zeolites 250, 1150, 1500, and 12000 had either disc or prismatic shapes that are typically associated with the MFI zeolite framework synthesized using tetrapropylammonium ions as the structure-directing agent [50].

The XRD patterns of the calcined samples are shown in Figure 1B. All of the samples have well-defined peaks that correspond to the monoclinic phase of MFI zeolites [51]. The lack of a broad peak in the 20° - 25° range (associated with amorphous x-ray diffraction) confirmed that the samples were crystalline[1]. The spectra of the two smaller zeolites, MFI 50 and MFI 120, had typical peak broadening associated with nanoparticles (Figure 1B, boxed regions) [49]. The average radius of MFI 50 and MFI 120, calculated using Equation (1), was found to be 20 nm and 50 nm, respectively (assuming a spherical geometry), and in good agreement with TEM images in Figure 1A.

3.1 Framework Water Capacity

3.1.1 Water Adsorption and Infiltration Experiments

In this section, we discuss a novel strategy where we combined water adsorption experiments (< 3 kPa) with high-pressure infiltration experiments (>1 MPa) to isolate the pre-adsorbed quantity of water and elucidate the actual framework

[1] Note that a small amount of localized distortions may be undetectable by standard XRD techniques, particularly for nano-sized crystals [52, 53]

capacity of MFI-type zeolites. The water uptake results for all the zeolites are shown in Figure 2A. The three larger zeolites, MFI 1150, 1500, and 12000, show similar water adsorption behavior that is indicative of low-uptake Type I isotherms [52], with ≈4 water molecules adsorbed per unit cell (N/UC) of zeolite at $P/P_o = 0.98$. Low-uptake Type I isotherms suggest a weak interaction between the adsorbent (zeolite) and adsorbate (water), which has been previously reported for these purely siliceous MFI zeolites [27, 33, 37]. While MFI 250 also exhibits a low-uptake Type I isotherm during the initial stages (partial pressure < 0.6, Figure 2A), the uptake rises substantially afterwards. This behavior is more indicative of a Type II isotherm [52] and a total of 17 N/UC was estimated to be adsorbed at a partial pressure of 0.98. MFI 120 and 50 show more typical behavior of Type II isotherms with a total adsorption of 22 and 57 N/UC, respectively.

The total adsorption at $P/P_o = 0.98$ was then used as the starting point for the high-pressure infiltration experiments (shown by the arrows in Figure 2A and 2B). Note that separate experiments (the details of which are elaborated in Section S.3 of the supplementary information) were performed to confirm that the total water inside the zeolites at the end of the adsorption experiments was the same as that during the start of high-pressure infiltration experiments. Little to no water entered into the zeolites after the adsorption experiments until the applied pressure exceeded ≈60 MPa. At this point, water infiltrated into the porous framework and subsequently saturated the zeolites once the pressure approached ≈130 MPa. This high-pressure infiltration behavior of water into MFI-type zeolites has been previously reported [11, 14, 46, 47, 53] and attributed to the decrease in both the

number of available water – water hydrogen bonds within the pore network (from ≈5 – 6 outside the zeolite to ≈2 within the pores) and to a lack of zeolite – water hydrogen bonding sites within the zeolite [46, 54-57][2]. The total capacity per unit cell (N_{tot}) at 160 MPa of applied pressure for all zeolites is reported in Table 3. MFI 1150, 1500, and 12000 have similar capacities of ≈35 ± 2 N/UC, which substantially increased as the crystal size decreased, with the maximum of ≈75 N/UC observed for MFI 50. These results also suggest that a majority of the water infiltration for smaller zeolites (MFI 50, 120 and 250) occurred in the low-pressure (≈2-3 kPa) adsorption regime. The percentage infiltration during the high pressure increased with increasing crystal dimension.

The results from these combined adsorption and infiltration experiments show a wide variation in both the water capacity and infiltration pressure of MFI-type zeolites, similar to what has been reported in literature (Table 1). However, both the textural porosity and localized distortions within the zeolite microstructure were found to significantly alter the framework capacity and misrepresent the actual infiltration behavior (as will be explained in Section 3.1.2).

3.1.2 Micropore Volume

The combined water adsorption and infiltration experiments demonstrated an increase in water capacity as the crystal dimensions decreased, suggesting apparent crystal size dependence of the water capacity of the zeolite network. This result was initially surprising since the different zeolites crystals used in this study were, in

[2] It should also be noted that the water fully evacuated the pores as the pressure was released, in agreement with previous studies [46, 56-59].

principle, composed of repeating three-dimensional unit cells, indicating that the framework water capacity (normalized with mass or per unit cell) should remain constant. In order to explain this discrepancy, we performed nitrogen sorption experiments to independently estimate the available micropore (framework) volume of the zeolites. It is well-known that nitrogen vapor completely saturates the framework micropores of these zeolites at low relative pressures ($P/P_o < 0.5$) [52]. As a result, any additional adsorption beyond P/P_o of 0.5 is indicative of both adsorption at the external crystal surface and in the available volume between crystals, both of which are associated with the textural porosity of the zeolite agglomerates [58, 59].

The micropore volume, calculated using the t-plot method (see Section S.4 of the supplementary information for details) for the larger MFI samples (250, 1150, 1500 and 12000) was found to ≈0.18 cm^3/g (Figure 3C and Table 3), which is in good agreement with previously reported values in literature [60]. However, a reduction of approximately 25% (Figure 3C and Table 3, V_f) in the framework volume was observed for the smaller sub-100 nm MFI zeolites (MFI 50 and 120). Furthermore, adsorption associated with the textural porosity considerably increased the amount of adsorbed nitrogen (V_{tot} in Table 3) for the nano-sized zeolite crystals (MFI 50, 120 and 250). These results suggest that the same textural porosity may have artificially increased the total water capacity as shown in Figure 2A. Assuming that the ratio of the total capacity (combined framework and textural)

to the framework capacity was the same for both nitrogen and water[3], the nitrogen sorption results were used to estimate the actual value of framework water capacity (Table 3). The analysis demonstrated that the role of the textural porosity on the water capacity was negligible and the framework water capacity was 35 ± 2 N/UC for the three larger zeolites (MFI 1150, 1500 and 12000). This result is expected considering the fact that the internal framework surface area was at least three orders of magnitudes larger than the estimated outer surface area. Interestingly, zeolite MFI 250 which had a total apparent water capacity of 43 N/UC, was also found to have a framework water capacity of 35 ± 2 N/UC. A framework capacity of 35 ± 2 N/UC for the four larger zeolites is in good agreement with the previously reported experimental results of Trzpit *et al*. [47] and Cailliez *et al*. [46]. However, most of the simulation-based results still overestimate the framework capacity by ≈20 – 40% [44, 46, 47, 53, 54], suggesting that the molecular interaction parameters currently used require further tuning.

Conversely, the analysis (Table 3) also indicated that the MFI 50 and 120 zeolites, despite having an apparent higher total capacity for both water and nitrogen compared to the larger MFI counterparts, actually exhibited a decrease in the framework water capacity of ≈45% to ≈50%. While this decrease in framework capacity of MFI zeolites with crystal diameters of 100 nm or less (which is more commonly investigated with nitrogen sorption) is in qualitative agreement with those found in literature (Table 4) [43, 47, 60-65] and the observed decrease in the

[3] The total capacity was determined at a partial pressure of 0.99 for the nitrogen adsorption experiments and at 160 MPa of applied pressure for the water adsorption/infiltration experiments

framework volume estimated *via* the nitrogen sorption presented earlier, the underlying mechanism for the reduction in framework volume/capacity is still unknown [52, 62, 66].

We hypothesize this decrease in the normalized framework volume to be indicative of a modification of the internal zeolite pore structure. While a long-range disordering of the microstructure was not observed as confirmed by XRD results in Figure 1B, localized distortion of the zeolite framework within the nanocrystals (known to be difficult to detect by XRD analysis [67, 68]) may have been present.

3.1.3 ^{29} Si MAS NMR spectroscopy

To investigate the presence of localized disorders (which were undetected by XRD) in the zeolite structure, we performed a more detailed investigation using ^{29}Si MAS NMR, a technique that is better suited to investigate the structure of zeolites and probe the existence of the non-crystalline material [67-69]. The structure and crystallinity of the zeolites were estimated by examining the spectra of the Q4 (Si-[(OSi)4]) groups that occurred in zeolites and other silica-based materials. Typically, well-crystallized MFI zeolites exhibit between 9 and 16 sharp peaks in the range of -108 to -118 ppm TMS chemical shift [47]. A decrease in number or sharpness of the peaks indicates an increase in the defect density or a reduction in crystallinity. For example, silica gels exhibit 1 – 3 broad peaks in the same frequency range, which is indicative of a disordered structure [69].

Figure 3B shows the NMR spectra collected for all samples. MFI 250, 1150, 1500 and 12000 had between 9 and 16 peaks and appeared to be well-crystallized. However, MFI 50 and 120 had fewer than 6 peaks and a significant lack of peak

sharpness, suggesting a loss in crystallinity. These results, when analyzed in conjunction with nitrogen sorption (Table 3) and water adsorption/infiltration (Figure 2 and Table 3) experiments, more clearly suggest that the decrease in the available framework capacity of the sub 100 nanometer diameter MFI 50 and 120 zeolites was indeed due to the incomplete crystallization of silica primary units during synthesis.

The incomplete crystallization of MFI primary units during synthesis can be explained by the growth mechanisms proposed by de Moor *et al*. [70]. They proposed that the primary units, which are sub 5 nm diameter amorphous silica particles, were absorbed into growing MFI zeolite crystals and subsequently crystallized into the zeolite structure during synthesis. However, due to the low crystallization temperatures (≤ 80°C) and slow crystal growth rates (≈1 nm per hour) of both MFI 50 and 120, it is plausible that some of these units did not completely crystallize during the synthesis process [67]. Furthermore, recent work has shown that if the nanoparticle synthesis occurs at temperatures of at least 170 °C, the full micropore volume (≈0.18 cm^3/g) can be recovered [14, 71].

3.3 Water Infiltration Pressure

The experimental results in Figure 2 showing significant water infiltration at low pressures (< 3 kPa), as demonstrated in the previous section, was attributed to the textural porosity and accordingly, did not correspond to the internal framework infiltration (Table 3). These results imply that, at most, only ≈15% of the framework volume was occupied with water at the end of the adsorption experiments and the

majority of the available framework volume was filled at high pressures (>60 MPa). The value of infiltration pressure was inferred from the maxima of the plot of differential water capacity (ΔN/UC) and applied pressure. As seen in Figure 4A, the infiltration pressure for all the zeolites was approximately the same and occurred between 95 – 100 MPa, which is in agreement with some previous studies [11, 46, 47, 53].

These results suggest that the crystallized internal framework of all the zeolites was approximately the same, with little to no difference in the internal surface chemistry and defect density. To further probe the internal surface chemistry, the low-pressure water adsorption isotherms were analyzed to quantify the defect density. The defects, which are in the form of silanol groups [33], are proposed to act as sites for water adsorption, thereby increasing the localized zeolite affinity for water. By analyzing the low (< 0.2) partial pressure water adsorption behavior (Figure 4B), the defect density for each zeolite was approximated (refer to Section S.4 of the supplementary information), as shown in Table 5 [37]. While the defect density for MFI 50 and 120 (which was estimated to be ≈0.45 defects per unit cell), was 6 – 10 times that of the larger zeolites, this estimated defect density indicates that, at most, only ≈0.5% of the silicon sites of each unit cell were defective for these nano-sized zeolites[4]. Previously, Trzpit *et al*. reported a reduction in the water infiltration pressure when defects were introduced into a previously perfect MFI zeolite, which contradicts the results

[4] No apparent peak associated with Q3 (or silanol groups) in the -100 ppm range existed in the recorded NMR spectra (Figure 3B), confirming that the quantity of the silanol defect density was relatively small (< 0.5% of the total sites available) [47].

presented here [47]. However, the defect densities studied in that work were higher (≈1 defect per unit cell), which could indicate that a threshold defect density needs to be attained before a noticeable decrease in the infiltration pressure can be observed. It should be noted that a rounding of the high-pressure infiltration curve was observed for the nanosized MFI 50 and 120 zeolites, which is in qualitative agreement with the results of Trzpit *et al.* in that an increasing defect density reduces the pronounced onset of the infiltration.

The combined results from these studies show that the purely siliceous MFI zeolites exhibit a 'hydrophobic' behavior where over 95 MPa is required to saturate the internal framework with water. These pressures are well in excess of the normal operating conditions associated with typical membrane operating pressures (for example, sea water reverse osmosis systems operate at pressures of 5.5 – 6.5 MPa [72]), which could explain the low water permeability of current zeolite-based membranes compared to polymeric-based membranes [12]. In order to address this challenge, we plan to artificially increase the internal defect density by varying the silicon to aluminum ratio to lower the water infiltration pressure [37, 47] and investigate the effects on water transport.

4. Conclusions

The effects of crystal size, morphology and synthesis procedure on the framework capacity and the associated micropore volume of purely siliceous MFI zeolites was systematically investigated using SEM, TEM, NMR, XRD, nitrogen sorption, water uptake and infiltration experiments. We demonstrated that the total

internal framework water capacity of fully crystallized MFI zeolites is 35 ± 2 water molecules per unit cell. In principle, no size effect on the total water capacity of the zeolites was inferred. However, an apparent decrease of up to 50% in internal framework water capacity and up to 25% in micropore volume for sub 100 nm diameter MFI zeolite crystals was found. Analysis of ^{29}Si MAS NMR spectra of the zeolites indicated this decrease in internal water capacity and micropore volume was due to an increase in localized disorder from the incomplete crystallization of MFI primary units during synthesis. The study also highlights the practical subtleties where the nano-sized MFI zeolites appear to have a larger water capacity ($\gg$35 water molecules per unit cell) due to water adsorption at the external surface and in inter-crystalline pores of the zeolite structure. Thus, for future experiments geared towards investigating the internal zeolite properties, we suggest an internal to external surface area ratio of at least 1000 be used to more accurately probe the internal pore network of the zeolites. The experimental quantification of the internal water capacity and the defect density as well as insight on the water infiltration pressure provided in this work can be utilized to help validate and improve upon the existing water and zeolite interaction models, as the current models still tend to overestimate the framework water capacity of MFI zeolites. Such advancements will allow better understanding of the transport mechanisms within the MFI zeolite pores, which can then be extended to other nanoscale materials as well.

Acknowledgements:

We thank Prof. Michael Tsapatsis (University of Minnesota) and Prof. Rohit Karnik (MIT) for helpful discussions and advice. We also thank Dr. Sonjong Hwang of the Solid State NMR group at the California Institute of Technology for performing the NMR experiments and analysis and Dr. Machteld Mertens (ExxonMobil, Belgium) for providing the large MFI 12000 zeolite sample. Additionally, we thank Pierce Hayward of the Mechanical Engineering Department at MIT, the staff at the Center for Materials Science and Engineering at MIT, and the staff at the Institute for Soldier Nanotechnologies at MIT for the training and use of equipment. This work was performed in part at the Center for Nanoscale Systems (CNS), a member of the National Nanotechnology Infrastructure Network (NNIN), which is supported by the National Science Foundation under NSF award no. ECS-0335765. CNS is part of Harvard University. This work was funded by the King Fahd University of Petroleum and Minerals in Dhahran, Saudi Arabia through the Center for Clean Water and Clean Energy at MIT and KFUPM. R.R. acknowledges fellowship support from Battelle's National Security Global Business.

References

[1] J. C. T. Eijkel and A. van den Berg, "The promise of nanotechnology for separation devices – from a top-down approach to nature-inspired separation devices," *Electrophoresis,* vol. 27, pp. 677-685, Mar 2006.

[2] W. Sparreboom, A. van den Berg, and J. Eijkel, "Transport in nanofluidic systems: a review of theory and applications," *New Journal of Physics,* vol. 12, p. 015004, 2010.
[3] W. Sparreboom, A. van den Berg, and J. C. T. Eijkel, "Principles and applications of nanofluidic transport," *Nature nanotechnology,* vol. 4, p. 713, Nov 08 2009.
[4] M. U. Niemann, S. S. Srinivasan, A. R. Phani, A. Kumar, D. Y. Goswami, and E. K. Stefanakos, "Nanomaterials for Hydrogen Storage Applications: A Review," *Journal of Nanomaterials,* vol. 2008, pp. 1-9, 2008.
[5] G. Reiss and A. Hütten, "Magnetic nanoparticles: Applications beyond data storage," *Nature Materials,* vol. 4, pp. 725-726, Oct 2005.
[6] C. Jianrong, M. Yuqing, H. Nongyue, W. Xiaohua, and L. Sijiao, "Nanotechnology and biosensors," *Biotechnology Advances,* vol. 22, pp. 505-518, Sep 2004.
[7] J. Holt, H. Park, Y. Wang, and M. Stadermann, "Fast mass transport through sub-2-nanometer carbon nanotubes," *Science,* 2006.
[8] C. Y. Won and N. R. Aluru, "Structure and dynamics of water confined in a boron nitride nanotube," *The Journal of Physical Chemistry C,* vol. 112, pp. 1812-1818, 2008.
[9] G. Hummer, J. C. Rasaiah, and J. P. Noworyta, "Water conduction through the hydrophobic channel of a carbon nanotube," *Nature,* vol. 414, pp. 188-190, 2001.
[10] H.-J. Wang, X.-K. Xi, A. Kleinhammes, and Y. Wu, "Temperature-Induced Hydrophobic-Hydrophilic Transition Observed by Water Adsorption," *Science,* vol. 322, pp. 80-83, Oct 03 2008.
[11] V. Eroshenko, R. Regis, M. Soulard, and J. Patarin, "Energetics: A new field of applications for hydrophobic zeolites," *Journal of the American Chemical Society,* vol. 123, pp. 8129-8130, 2001.
[12] T. Humplik, J. Lee, S. C. O'Hern, B. A. Fellman, M. A. Baig, S. F. Hassan*, et al.*, "Nanostructured materials for water desalination," *Nanotechnology,* vol. 22, p. 292001, Jul 17 2011.
[13] X. Gong, J. Li, H. Lu, R. Wan, J. Li, J. Hu*, et al.*, "A charge-driven molecular water pump," *Nature nanotechnology,* 2007.
[14] M. Trzpit, M. Soulard, and J. Patarin, "Water intrusion in mesoporous silicalite-1: An increase of the stored energy," *Microporous and Mesoporous Materials,* vol. 117, pp. 627-634, 2009.
[15] J. Rasaiah, S. Garde, and G. Hummer, "Water in Nonpolar Confinement: From Nanotubes to Proteins and Beyond*," *Annual Reviews,* 2008.
[16] C. Y. Lee, W. Choi, J.-H. Han, and M. S. Strano, "Coherence Resonance in a Single-Walled Carbon Nanotube Ion Channel," *Science,* vol. 329, pp. 1320-1324, Sep 10 2010.
[17] C. Ho, R. Qiao, J. Heng, A. Chatterjee, R. Timp, N. Aluru*, et al.*, "Electrolytic transport through a synthetic nanometer-diameter pore," *Proceedings of the National Academy of Sciences,* vol. 102, pp. 10445-10450, 2005.
[18] Y. Qiao, L. Liu, and X. Chen, "Pressurized Liquid in Nanopores: A Modified Laplace-Young Equation," *Nano Lett,* 2009.

[19] M. R. Powell, L. Cleary, M. Davenport, K. J. Shea, and Z. S. Siwy, "Electric-field-induced wetting and dewetting in single hydrophobic nanopores," *Nature nanotechnology,* vol. 6, pp. 798-802, Oct 30 2011.
[20] Z. Siwy, I. Kosińska, A. Fuliński, and C. Martin, "Asymmetric diffusion through synthetic nanopores," *Physical Review Letters,* vol. 94, p. 48102, 2005.
[21] G. Cicero, J. C. Grossman, E. Schwegler, F. Gygi, and G. Galli, "Water confined in nanotubes and between graphene sheets: A first principle study," *Journal of the American Chemical Society,* vol. 130, p. 1871, 2008.
[22] D. Cohen-Tanugi and J. C. Grossman, "Water Desalination across Nanoporous Graphene," *Nano Letters,* vol. 12, pp. 3602-3608, Jul 2012.
[23] J. Čejka, H. van Bekkum, A. Corma, and F. Schueth, *Introduction to Zeolite Molecular Sieves*: Elsevier Science, 2007.
[24] Y. Liu and X. Chen, "High permeability and salt rejection reverse osmosis by zeolite nano-membrane," *Phys Chem Chem Phys,* 2013.
[25] L. Li, J. Dong, T. Nenoff, and R. Lee, "Desalination by reverse osmosis using MFI zeolite membranes," *Journal of Membrane Science,* vol. 243, pp. 401-404, 2004.
[26] M. Drobek, C. Yacou, J. Motuzas, A. Julbe, L. Ding, and J. C. Diniz da Costa, "Long term pervaporation desalination of tubular MFI zeolite membranes," *Journal of Membrane Science,* vol. 415-416, pp. 816-823, Oct 2012.
[27] N. Chen, "Hydrophobic properties of zeolites," *The Journal of Physical Chemistry,* vol. 80, pp. 60-64, 1976.
[28] M. G. k. Ahunbay, "Monte Carlo Simulation of Water Adsorption in Hydrophobic MFI Zeolites with Hydrophilic Sites," *Langmuir,* vol. 27, pp. 4986-4993, May 19 2011.
[29] V. Bolis, C. Busco, and P. Ugliengo, "Thermodynamic Study of Water Adsorption in High-Silica Zeolites," *The Journal of Physical Chemistry B,* vol. 110, pp. 14849-14859, Aug 2006.
[30] F. Cailliez, G. Stirnemann, A. Boutin, I. Demachy, and A. H. Fuchs, "Does water condense in hydrophobic cavities? A molecular simulation study of hydration in heterogeneous nanopores," *The Journal of Physical Chemistry C,* vol. 112, pp. 10435-10445, 2008.
[31] P. Demontis, J. Gulín-González, M. Masia, and G. B. Suffritti, "The behaviour of water confined in zeolites: molecular dynamics simulations versus experiment," *Journal of Physics: Condensed Matter,* vol. 22, p. 284106, Jul 21 2010.
[32] A. Han and Y. Qiao, "Infiltration of liquid water in an acid-leached zeolite," *Journal of Materials Research,* 2007.
[33] A. Jentys, G. Warecka, M. Derewinski, and J. Lercher, "Adsorption of water on ZSM 5 zeolites," *The Journal of Physical Chemistry,* vol. 93, pp. 4837-4843, 1989.
[34] T. Masuda, S. Otani, T. Tsuji, M. Kitamura, and S. R. Mukai, "Preparation of hydrophilic and acid-proof silicalite-1 zeolite membrane and its application to selective separation of water from water solutions of concentrated acetic acid by pervaporation," *Separation and purification technology,* vol. 32, pp. 181-189, 2003.

[35] R. Valiullin, J. Kärger, K. Cho, M. Choi, and R. Ryoo, "Dynamics of water diffusion in mesoporous zeolites," *Microporous and Mesoporous Materials,* vol. 142, pp. 236-244, Jul 2011.
[36] S. A. Zygmunt, L. A. Curtiss, L. E. Iton, and M. K. Erhardt, "Computational Studies of Water Adsorption in the Zeolite H-ZSM-5," *The Journal of Physical Chemistry,* vol. 100, pp. 6663-6671, Feb 1996.
[37] D. Olson, W. Haag, and W. Borghard, "Use of water as a probe of zeolitic properties: interaction of water with HZSM-5," *Microporous and Mesoporous Materials,* vol. 35, pp. 435-446, 2000.
[38] H. Thamm, "Adsorption site heterogeneity in silicalite: a calorimetric study," *Zeolites,* vol. 7, pp. 341-346, Jul 1987.
[39] A. Filippov, S. V. Dvinskikh, A. Khakimov, M. Grahn, H. Zhou, I. Furo*, et al.*, "Dynamic properties of water in silicalite-1 powder," *Colloids and Surfaces,* vol. 30, pp. 1022-1031, Sep 2012.
[40] M. Arı, M. Ahunbay, M. Yurtsever, and A. Erdem, "Molecular Dynamics Simulation of Water Diffusion in MFI-Type Zeolites," *J. Phys. Chem. …,* 2009.
[41] J. Caro, S. Hŏcevar, J. Kärger, and L. Riekert, "Intracrystalline self-diffusion of H2O and CH4 in ZSM-5 zeolites," *Colloids and Surfaces,* vol. 6, pp. 213-216, Jun 1986.
[42] P. Demontis, H. Jobic, and M. Gonzalez, "Diffusion of water in zeolites NaX and NaY studied by quasi-elastic neutron scattering and computer simulation," *The Journal of Physical …,* 2009.
[43] K. Zhang, R. P. Lively, M. E. Dose, L. Li, W. J. Koros, D. M. Ruthven*, et al.*, "Diffusion of water and ethanol in silicalite crystals synthesized in fluoride media," *Microporous and Mesoporous Materials,* vol. 170, pp. 259-265, May 2013.
[44] C. E. Ramachandran, S. Chempath, L. J. Broadbelt, and R. Q. Snurr, "Water adsorption in hydrophobic nanopores: Monte Carlo simulations of water in silicalite," *Microporous and Mesoporous Materials,* vol. 90, pp. 293-298, 2006.
[45] A. Özgür YazaydIn and R. Thompson, "Molecular simulation of water adsorption in silicalite: Effect of silanol groups and different cations," *Microporous and Mesoporous Materials,* vol. 123, pp. 169-176, 2009.
[46] F. Cailliez, M. Trzpit, M. Soulard, I. Demachy, A. Boutin, J. Patarin*, et al.*, "Thermodynamics of water intrusion in nanoporous hydrophobic solids," *Physical Chemistry Chemical Physics,* vol. 10, pp. 4817-4826, 2008.
[47] M. Trzpit, M. Soulard, J. Patarin, N. Desbiens, F. Cailliez, A. Boutin*, et al.*, "The effect of local defects on water adsorption in silicalite-1 zeolite: a joint experimental and molecular simulation study.," *Langmuir: the ACS journal of surfaces and colloids,* vol. 23, p. 10131, 2007.
[48] S. C. Maroo, T. Humplik, T. Laoui, and E. N. Wang, "Water Transport in Sub-nanometer MFI Zeolites for Efficient Water Desalination," in *ASME 2012 3rd Micro/Nanoscale Heat & Mass Transfer International Conference*, Atlanta, Georgia, 2012.
[49] A. Patterson, "The Scherrer Formula for X-Ray Particle Size Determination," *Physical Review,* vol. 56, pp. 978-982, Nov 1939.

[50] Z. Lai, M. Tsapatsis, and J. Nicolich, "Siliceous ZSM-5 Membranes by Secondary Growth of b-Oriented Seed Layers," *Advanced Functional Materials,* vol. 14, 2004.
[51] D. Olson, G. Kokotailo, S. Lawton, and W. Meier, "Crystal-structure and structure-related properties of ZSM-5," *Journal Of Physical Chemistry,* vol. 85, pp. 2238-2243, 1981.
[52] J. Rouquerol, F. Rouquerol, and K. S. W. Sing, *Absorption by Powders and Porous Solids*: Academic Press, 1998.
[53] A. Lella, N. Desbiens, A. Boutin, and I. Demachy, "Molecular simulation studies of water physisorption in zeolites," *Physical Chemistry Chemical Physics,* 2006.
[54] N. Desbiens, A. Boutin, and I. Demachy, "Water condensation in hydrophobic silicalite-1 zeolite: A molecular simulation study," *The Journal of Physical Chemistry B,* vol. 109, pp. 24071-24076, 2005.
[55] N. Giovambattista, P. G. Debenedetti, and P. J. Rossky, "Hydration behavior under confinement by nanoscale surfaces with patterned hydrophobicity and hydrophilicity," *The Journal of Physical Chemistry C,* vol. 111, pp. 1323-1332, 2007.
[56] T. Karbowiak, C. Paulin, A. Ballandras, G. Weber, and J.-P. Bellat, "Thermal Effects of Water Intrusion in Hydrophobic Nanoporous Materials," *Journal of the American Chemical Society,* vol. 131, pp. 9898-+, 2009.
[57] J. Zhao, P. Culligan, J. Germaine, and X. Chen, "Experimental Study on Energy Dissipation of Electrolytes in Nanopores," *Langmuir,* 2009.
[58] H. Chen and Y. Wang, "Preparation of MCM-41 with high thermal stability and complementary textural porosity," *Ceramics International,* vol. 28, pp. 541-547, 2002.
[59] T. R. Pauly, Y. Liu, T. J. Pinnavaia, S. J. Billinge, and T. P. Rieker, "Textural mesoporosity and the catalytic activity of mesoporous molecular sieves with wormhole framework structures," *Journal of the American Chemical Society,* vol. 121, pp. 8835-8842, 1999.
[60] M. B. Kenny and K. Sing, "The Hydrophobicity of Silicalite and ZSM-5," *Chemistry & Industry,* pp. 39-40, 1990.
[61] S.-S. Kim, J. Shah, and T. J. Pinnavaia, "Colloid-Imprinted Carbons as Templates for the Nanocasting Synthesis of Mesoporous ZSM-5 Zeolite," *Chem. Mater,* vol. 15, pp. 1664-1668, May 2003.
[62] C.-Y. Hsu, A. S. T. Chiang, R. Selvin, and R. W. Thompson, "Rapid Synthesis of MFI Zeolite Nanocrystals," *The Journal of Physical Chemistry B,* vol. 109, pp. 18804-18814, Oct 2005.
[63] T. Babeva, R. Todorov, S. Mintova, and T. Yovcheva, "Optical properties of silica MFI doped acrylamide-based photopolymer," *Journal of Optics A,* 2009.
[64] G. Majano, A. Darwiche, S. Mintova, and V. Valtchev, "Seed-Induced Crystallization of Nanosized Na-ZSM-5 Crystals," *Ind. Eng. Chem. Res,* vol. 48, pp. 7084-7091, Aug 05 2009.
[65] J. Aguado, D. P. Serrano, J. M. Escola, and J. M. Rodriguez, "Low temperature synthesis and properties of ZSM-5 aggregates formed by ultra-small

nanocrystals," *Microporous and Mesoporous Materials,* vol. 75, pp. 41-49, 2004.
[66] E. E. Mallon, M. Y. Jeon, M. Navarro, A. Bhan, and M. Tsapatsis, "Probing the Relationship between Silicalite-1 Defects and Polyol Adsorption Properties," *Langmuir,* vol. 29, pp. 6546-6555, Jul 04 2013.
[67] K. F. M. G. J. Scholle, W. S. Veeman, P. Frenken, and G. P. M. van der Velden, "Characterization of intermediate TPA-ZSM-5 type structures during crystallization," *Applied Catalysis,* vol. 17, pp. 233-259, Aug 1985.
[68] W. Zhang, X. Bao, X. Guo, and X. Wang, "A high‐resolution solid‐state NMR study on nano‐structured HZSM‐5 zeolite," *Catalysis Letters,* vol. 60, pp. 89-94, 1999.
[69] R. Dupree, D. Holland, P. W. McMillan, and R. F. Pettifer, "The structure of soda-silica glasses: A mas NMR study," *Journal of Non-Crystalline Solids,* vol. 68, pp. 399-410, Nov 1984.
[70] P.-P. E. de Moor, T. P. Beelen, and R. A. van Santen, "In situ observation of nucleation and crystal growth in zeolite synthesis. A small-angle X-ray scattering investigation on Si-TPA-MFI," *The Journal of Physical Chemistry B,* vol. 103, pp. 1639-1650, 1999.
[71] D. P. Serrano, R. A. Garcia, M. Linares, and B. Gil, "Influence of the calcination treatment on the catalytic properties of hierarchical ZSM-5," *Catalysis Today,* vol. 179, pp. 91-101, Jan 5 2012.
[72] C. Fritzmann, J. Löwenberg, T. Wintgens, and T. Melin, "State-of-the-art of reverse osmosis desalination," *Desalination,* vol. 216, pp. 1-76, 2007.
[73] M. Ahunbay, "Monte Carlo Simulation of Water Adsorption in Hydrophobic MFI Zeolites with Hydrophilic Sites," *Langmuir,* 2011.

Tables

Table 1. Infiltration pressure and water capacity into MFI zeolites pores compiled from various studies. (S) indicates simulation-based results and (E) indicates experimentally measured quantities. For consistency, the framework capacity is taken at a value of 160 MPa to correspond to our experimental conditions of this study. Note the large variation in the capacity and infiltration pressure amongst the reported values. Olson *et al*. [37] did not investigate the infiltration pressure.

Source	Framework Capacity (N/UC)	Infiltration Pressure (MPa)
Trzpit *et al.* [47]	34 - 37 (E), 41 (S)	75 - 125 (S, E)
Cailliez *et al*. [46]	35 (E), 40 (S)	80 (E), 120 (S)
Desbiens *et al.* [54]	39 - 45 (S)	0.01 - 100 (S)
Ahunbay *et al*. [73]	35 - 37 (S)	0.01 (S)
Lella *et al.* [53]	39 - 41 (S)	80 - 120 (S)
Ramachandran *et al.* [44]	57 (S)	0.001 - 0.003 (S)
Olson *et al.* [37]	53 (E)	n/a

Table 2. Synthesis conditions for the various MFI zeolites. The composition refers to the molar ratio of TEOS:TPAOH:H_2O used. The characteristic dimension for each zeolite is the crystal volume to external surface area ratio and is given in units of nanometers. MFI 12000 was procured from Exxon Mobil, Machelen, Belgium.

Zeolite	Composition	Conditions	Characteristic Dimension (nm)
MFI 50	25 : 9 : 450	60 °C for 168 hours	7
MFI 120	25 : 9 : 450	80 °C for 196 hours	18
MFI 250	4 : 1 : 72	80 °C for 90 minutes, 180 °C for 30 minutes	40
MFI 1150	5 : 1 : 500	160 °C for 5 hours	175
MFI 1500	5 : 1 : 1000	160 °C for 5 hours	235
MFI 12000	n/a	n/a	1800

Table 3. Calculated micropore volume (V_f) and estimated internal water capacity (N_f) of MFI zeolites. V_{tot} and N_{tot} are the total adsorption/infiltration quantities determined at $P/P_o = 0.99$ for nitrogen sorption and P = 160 MPa for water infiltration, respectively. The ratio (R) is of the total nitrogen adsorption (combined framework and textural) to the framework nitrogen adsorption, which was then used to estimate the internal water capacity. Note the significant decrease in internal water capacity for MFI 50 and 120, which is attributed to the incomplete crystallization of incorporated primary units. MFI 250, 1150, 1500 and 12000 have comparable values for the internal capacity, and are within the uncertainty of the infiltration experiments.

Zeolite	Nitrogen Sorption			Water Adsorption + Infiltration		
	V_f (cm^3/g)	V_{tot} (cm^3/g)	R	N_{tot} (N/UC)	$N_f = N_{tot}/R$ (N/UC)	% decrease in N_f
MFI 50	0.136	0.613	4.51	75	17	≈50%
MFI 120	0.137	0.316	2.31	43	19	≈45%
MFI 250	0.178	0.222	1.25	43	35	≈0%
MFI 1150	0.173	0.178	1.03	34	33	≈0%
MFI 1500	0.185	0.193	1.04	35	34	≈0%
MFI 12000	0.177	0.179	1.01	35	35	≈0%

Table 4. Summary of past work highlighting reduction in measured micropore volume for nano-sized MFI-type zeolites. Note that the typical range for the micropore volume for crystalline MFI-type zeolites determined with nitrogen sorption is between 0.18 and 0.2 cm^3/g.

Source	Crystal Size (nm)	Pore Volume (cm^3/g)
Kim *et al.* [61]	13	0.081
Kim *et al.* [61]	22	0.090
Hsu *et al.* [62]	40	0.110
Kim *et al.* [61]	42	0.138
Babeva *et al.* [63]	70	0.120
Majano *et al.* [64]	80	0.130
Kim *et al.* [61]	90	0.115
Aguado *et al.* [65]	10-100	0.140
Trzpit *et al.* [47]	20000	0.185
Zhang *et al.* [43]	70000	0.196
Kenny and Sing [60]	not given	0.190

Table 5. Calculated defect densities of MFI zeolites obtained by extrapolating the intercept from the water adsorption isotherms (see supplementary materials, Figure S3A). MFI 50 and 120 exhibited slightly higher defect densities, as only 0.5% of the total available silicon sites with the unit cell were defective.

Zeolite	Defects/UC
MFI 50	0.448
MFI 120	0.450
MFI 250	0.063
MFI 1150	0.043
MFI 1500	0.048
MFI 12000	0.078

Figures

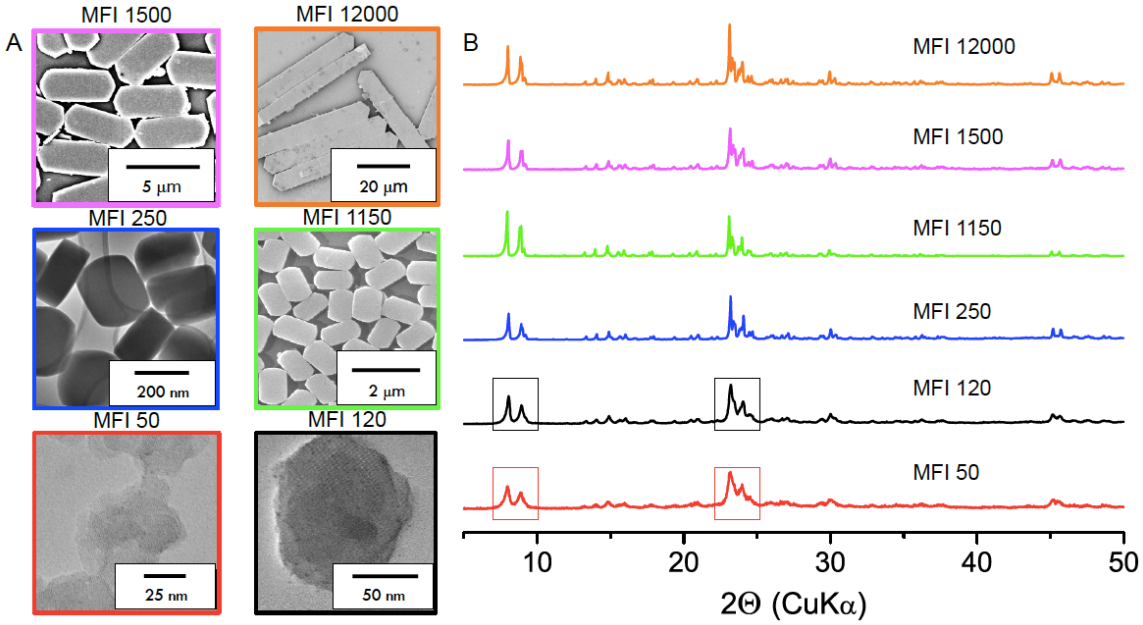

Figure 1. Electron microscopy (A) and x-ray diffraction (B) analysis of MFI zeolites. TEM was used for the nano-sized MFI 50, 120 and 250 zeolites while SEM utilized for the micron-sized MFI 1150, 1500 and 12000 zeolites. The XRD patterns for each zeolite sample matched well with the monoclinic phase of MFI zeolites. The boxes for MFI 50 and 120 highlight the diffraction peaks that were broadened due to diffraction of the nanoparticles themselves. These peaks were used to quantify the size of MFI 50 and 120.

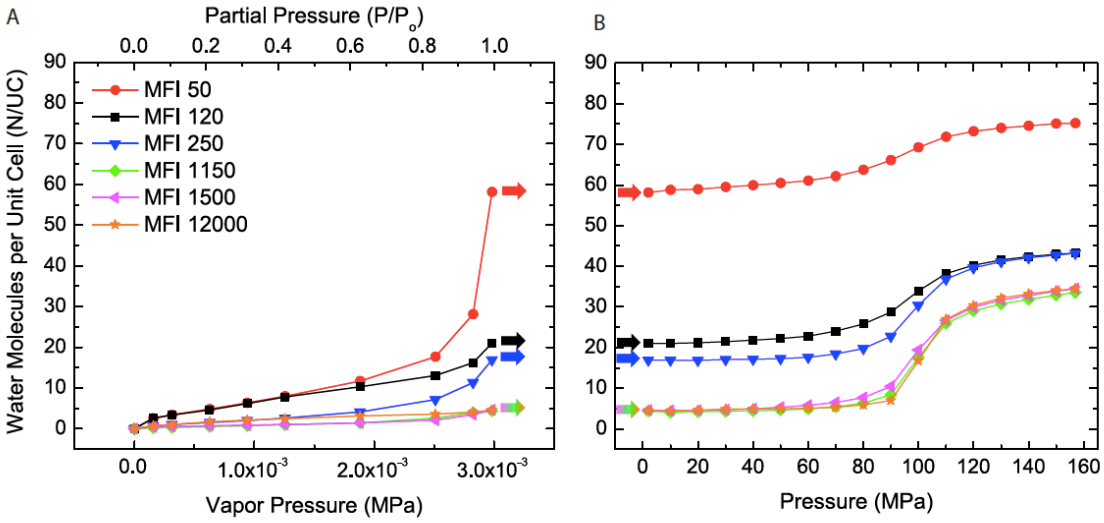

Figure 2. Combined water adsorption and infiltration isotherms for MFI-type zeolites **A.** Water adsorption isotherms at 25°C for varying crystal sizes of MFI zeolites. The ordinate corresponds to the amount of water adsorbed per unit cell of the zeolite and the abscissa corresponds to the vapor pressure of water (the partial pressure is also plotted for reference). The measurement error was less than the symbol size. The increase in adsorption at higher pressure for the nano-sized zeolites is indicative of capillary condensation in the pores of the crystal agglomerates. **B.** Experimental pressure infiltration curves of water into the six zeolites. The ordinate is the calculated amount of water entering per unit cell of the zeolite where the starting point was shifted by the capacity at the end of adsorption experiments in A. The abscissa is the experimentally measured applied pressure. The error associated with displacement was ± 2 N/UC. The arrows help connect the starting point for each plot, which corresponds to the infiltrated water at ≈98% RH (P/P_o = 0.98) from the adsorption experiments. The final measured capacity for MFI 50, 120 and 250 overestimated the internal capacity due to the effects of the textural porosity. This surface effect was negligible for MFI 1150, 1500 and 12000, and therefore these measurements indicated the correct total internal water capacity associated with MFI zeolites.

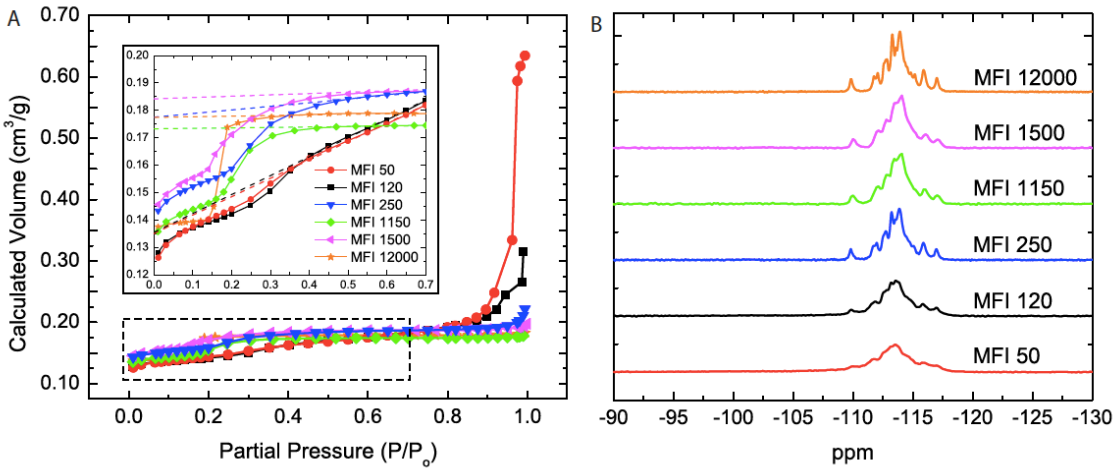

Figure 3. Nitrogen sorption and NMR spectra of MFI-type zeolites **A.** Nitrogen adsorption isotherms with the ordinate corresponding to the calculated pore volume and the abscissa corresponding to the partial pressure of nitrogen at 77 K. The t-plot pore volume (Table 3) was estimated by extrapolating the y-intercept from a linear fit in the partial pressure regions of 0.5 – 0.7 Inset shows a magnified view of the black dotted box with the dashed lines showing the linear fit. There was a ≈25% decrease in the micropore volume of MFI 50 and 120 compared to the larger MFI 250, 1150, 1500 and 12000 samples. **B.** ^{29}Si MAS NMR spectra for varying crystal sizes of MFI zeolites. Note that the curves have been arbitrarily shifted in the y direction for clarity. The decrease in the number of peaks as well as the peak sharpness seen in the spectra of MFI 50 and 120 indicates an increase in localized disorder, which was a result of incomplete crystallization of amorphous primary units during synthesis. The presence of the amorphous material explains the decrease in the measured micropore volume.

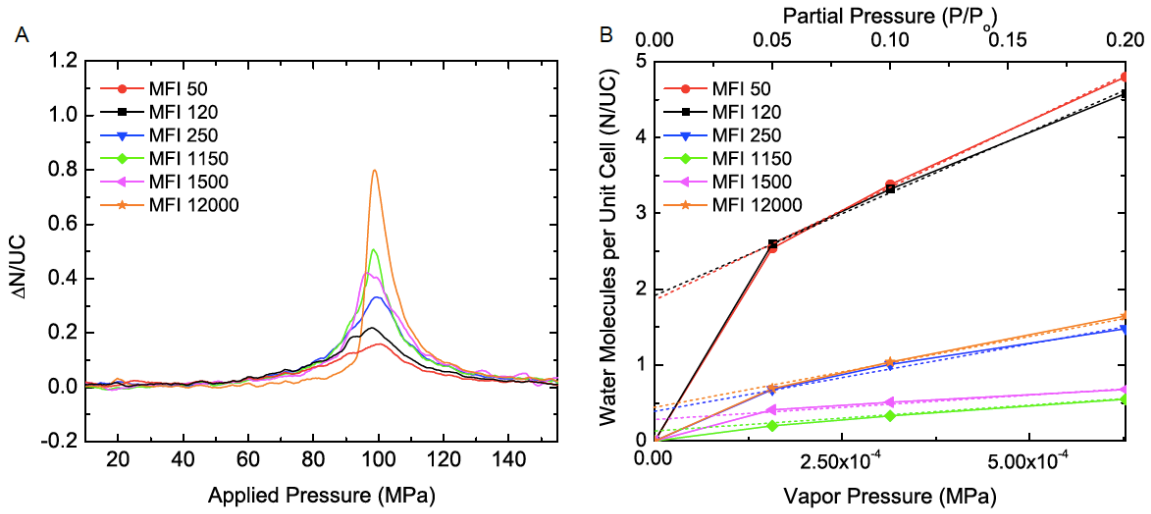

Figure 4. Defect density effects on the infiltration pressure and low-pressure water uptake. **A**. The change in infiltrated amount of water into the zeolites as a function of applied pressure. The infiltration pressure corresponds to the maximum for each curve. Note that the infiltration pressure for all zeolites studied here was between 95 – 100 MPa. **B.** A magnified view of the low partial pressure water uptake isotherms highlighting the difference in the low uptake data as well as the approximate linear slopes (dashed lines) obtained to calculate the defect density.

Supplementary Information

S.1 Synthesis details

Measured amounts of TEOS, TPAOH, and H_2O were mixed at room temperature and stirred for at least 12 hours to obtain a clear solution. The solutions were then transferred into their appropriate vessel for synthesis. For hydrothermal treatment, a 45 mL PTFE-lined stainless steel autoclave (Parr, Inc) was used and was rotated at ~ 100 RPM inside of an oven (BlueM, Thermal Product Solutions) at the desired temperature. For microwave synthesis, a Kevlar-lined PTFE vessel (HP-500, CEM) was used with a MARS 5 (CEM) microwave oven. For the smallest zeolites, PTFE tubes (VWR) were placed in a temperature-controlled bath (PolyScience) and held at temperature without agitation. After synthesis, the zeolites were recovered by centrifugation and washed with deionized water until the pH of the solution was ~ 9. This was followed by drying at 60 °C and calcination under air at 550 °C for three hours to remove the organic template. MFI-F was kindly provided by Dr. Machteld Mertens (ExxonMobil, Machelen, Belgium).

S.2 Pressure vessel design and experimental operation

The pressure vessel was made of type-304 stainless steel (McMaster-Carr) and used a two-piston setup within a cylinder (see Figure S1). The vessel was sealed using polyurethane o-rings (90 Shore A, McMaster-Carr) and secured with glass-filled PTFE backup rings. 10 mL of deionized water (class 2, VWR) and between 1 -2.5 g

of zeolite (the amount was varied to ensure that the water capacity was independent of the zeolite amount and repeatable) were sealed within the vessel. We machined the pressure vessel from 304 stainless steel-due to its high strength, corrosion resistance and machinability. The inner diameter of the pressure was made to be 0.502" and polished with burnishing tools. The pistons were also made from 304 stainless and had grooves machined into them to hold two glass-filled PTFE backup rings and a urethane (90 Shore A hardness) o-ring. The other dimension of the o-ring was 0.504" so it had to compress slightly to fit into the pressure vessel. This level of precision was required so that the vessel would not leak under high (> 100 MPa) pressure. Polymer o-rings usually are not used for this type of setup, however, we did not observe leaking during the experiments. O-rings and backup rings were replaced after every experiment to decrease the chance of o-ring failure.

The pressure vessel needed to be interfaced with an apparatus to apply a force and monitor displacement. For our experiments, we used an Instron 5582 running the BlueHill 2 software. The Instron is capable of applying loads of 100 kN (although we only needed 20 kN). To determine the infiltration behavior into the pores, we used the 'compliance correct' feature on the software. The compliance we corrected for was a control sample of 10 mL of water. Since every experiment used 10 mL of water, we used to software to remove this displacement from the experiments. Therefore, any additional displacement (due to water infiltrating into the zeolite pores) would be recorded as the only displacement in the data. This

removes time-consuming post processing of the raw data and largely removes a source for any error in the data.

For the experiments, we used 1.0 g to 2.5 g of zeolites immersed in class 2 deionized water (VWR). A specific mass of zeolite was weighed and poured into a glass beaker containing 10 mL of the deionized water. The solution was mixed for ~30 minutes with a magnetic stir rod at 200 RPM to create a well-dispersed mixture. The solution was then transferred to the pressure vessel. Great care was taken so that macro scale air bubbles (and air in general) were not introduced into the vessel. The vessel was then sealed with a second piston and aligned so that the solution is approximately in the center of the vessel. The vessel subseuqnetly placed into a holder to maintain an upright position and transferred to the Instron 5582. A schematic of the actual vessel used as well as a picture of the experimental setup is shown in Figure S1.

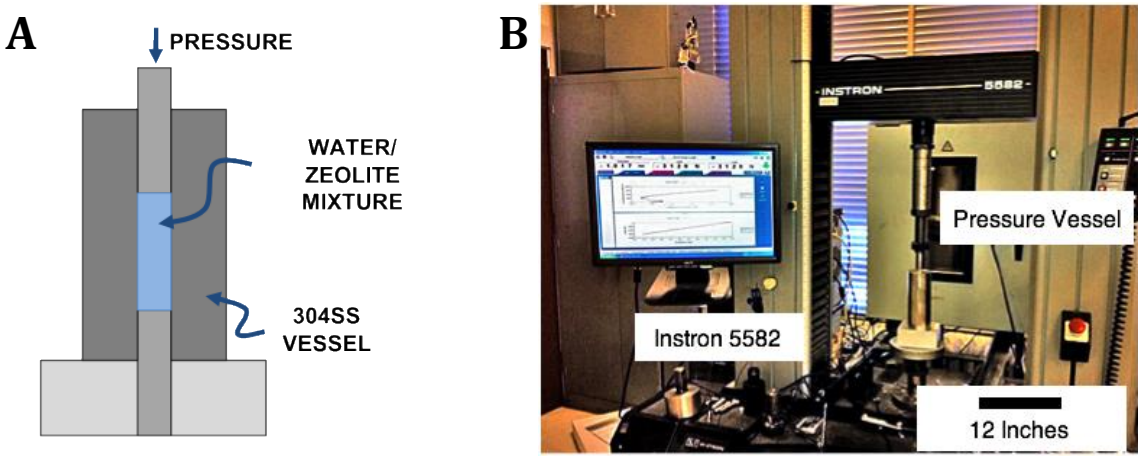

Figure S1. A. Schematic of the two-piston pressure vessel used for infiltration experiments. B. Picture of the Instron 5582 with pressure vessel loaded into the apparatus.

After the completion of the compression, the pressure was released and the vessel returned to the initial position confirming the previous observations where water completely evacuated the pores. Consistency in the experimental procedure and repeatability of the data was confirmed by running four to six experiments each. The control displacement would be subtracted from the experimental, which would therefore subtract the compliance of the mechanical test apparatus, the vessel, and the zeolites. To convert to a number of water molecules, the net volume is multiplied by the density of water at the corresponding pressure (found from NIST tables) and then divided by the mass of a water molecule (3×10^{-23} g).

S.3 Confirming the Starting Value of Infiltration Experiments

To determine if extra water entered into the zeolite as it immersed into liquid water, an experimental setup depicted in Figure S2 was utilized. Initially, a known mass of zeolites, enough to completely fill an aluminum crucible with a known volume (V_{tot}, 160 µL) (DSC Al crucible, Mettler Toledo) was dried at 400 °C under air and the total dry mass of the zeolites ($M_{zeolite}$) was recorded. Having computed the dry mass of the zeolites, the intercrystalline volume (V_{inter}) was calculated by subtracting the zeolite volume ($V_{zeolite,dry}$) from the total volume of the crucible (V_{tot}).

$$V_{tot} - V_{zeolite,dry} = V_{inter}\ ;\ where\ V_{zeolite,dry} = \frac{M_{zeolite}}{\rho_{zeolite}}$$

Next, the samples were exposed to a 98% RH environment in Q5000SA vapor sorption analyzer and the measured increase in mass ($M_{water,ads}$) was used to

calculate the total adsorbed water within the zeolites. The calculated adsorbed water per unit mass was confirmed to be in agreement with the numbers reported in Figure 2A. Since the effect of adsorption on the external surface area and capillary condensation in the intercrystalline pores was negligible for these larger zeolites (Figure 3a), we assumed all of the adsorbed water to be within the zeolite pores, not changing the previously computed intercrystalline volume (V_{inter}). Next, enough liquid water mass required to completely fill the intercrystalline volume was introduced *via* a pipette into the aluminum crucible containing the water-saturated zeolites and the extra mass was recorded using an mass balance (Discovery, OHAUS) (with a resolution of 10 μg). This procedure mimicked the process of introducing the water saturated zeolites (at 98% RH) into the water bath of the pressure vessel used in the infiltration measurements. The volume occupied by the additional water added *via* the pipette (assuming a bulk density of 1 g/cm^3) was found to match the previously computed intercrystalline volume (V_{inter}), confirming no additional water infiltrated into the zeolite and thus justifying the use of the last data point in Figure 2A as the starting point for Figure 2B.

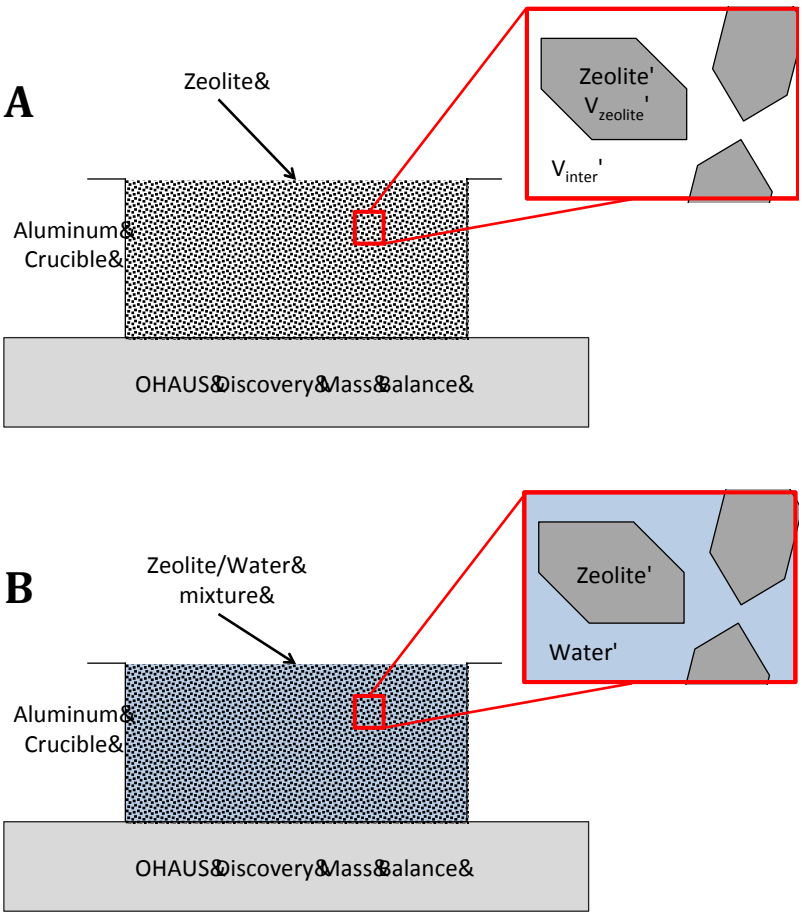

Figure S2. Schematic of experimental setup used to determine if additional water entered into the zeolites after the adsorption experiments but prior to the infiltration experiments. **A)** Schematic before water was added, highlighting the available volume of the zeolite and intercrystalline space. **B)** Schematic after water was added, showing that the full intercrystalline space was filled with water.

S.4 Defect Density and Micropore Volume Calculations

Following the procedure of Olson *et al.,* the defect density can be approximated by extrapolating a linear fit in the low partial pressure ranges, highlighted in Figure 4B, and finding the y-axis intercept (which correlates to a number of water molecules per unit cell). The defect density was calculated by assuming that each defect adsorbs ~ 4 water molecules at low partial pressures

(therefore, the defect density is ¼ of the number of adsorbed molecules at hypothetic vacuum). The quantified defect density is in Table 3.

For the micropore volume, a similar extrapolation procedure was used. As highlighted in the inset of Figure 3A, a linear fit in the partial pressure range of 0.5 – 0.7 in the nitrogen sorption data was applied with the corresponding y-intercept as the available micropore volume.

S.5 Estimation of the Water Infiltration Pressure

To investigate the infiltration pressure, the change in the infiltrated water capacity as a function of pressure was plotted (see Figure 4A). We defined the infiltration pressure as the pressure at which the maximum amount of water filled into the zeolite pores which corresponded to the maximum in the curves shown in Figure S4. The data was smoothed (averaged over 10 data points or ~ 3 MPa in pressure range).